Static magnetometer suitable for weakly permeable magnetic fluids

Highlighting method of anisotropy assessment

Mickaël Petit[1], **Afef Kedous-Lebouc**[2], **Olivier Geoffroy**[2], **Yvan Avenas**[2], **Wahid Cherief**[2]

1. SATIE, ENS Cachan - CNAM - Université de Cergy Pontoise - CNRS UMR8029
61, Avenue du Président Wilson, 94230 Cachan, France
mickael.petit@satie.ens-cachan.fr

2. Univ. Grenoble Alpes, CNRS, G2Elab, 38000 Grenoble, France
(afef.lebouc; olivier.geofroy; yvan.avenas; wahid.cherief)@g2elab.grenoble-inp.fr

ABSTRACT. *Ferrofluids have a highly nonlinear magnetic behavior. Moreover, their colloidal nature may, in certain circumstances, make anisotropic by forming chains. A fine characterization of these liquids is essential. However, conventional measurement methods, setting in motion the samples tested are ineffective against these materials. The following article highlights a static method to draw the characteristic J(H) of a sample of ferrofluid. It consists in four parts. The first describes the measurement principle and the mathematical method involved. The second part of the article shows how the magnetometer was designed, implemented and calibrated. In the third part, the magnetometer is tested on a solid sample slightly permeable. Down results obtained are compared to measurement by extraction. Finally, a fourth part shows thanks to a numerical simulation that the device is able to highlight the isotropic or anisotropic nature of the test sample.*

RÉSUMÉ. *Les ferrofluides ont un comportement magnétique fortement non linéaire. De plus, leur nature colloïdale peut, dans certaines conditions, les rendre anisotrope par formation de chaînes. Une caractérisation fine de ces liquides est donc indispensable. Cependant les méthodes classiques de mesure, mettant en mouvement les échantillons testés, sont inefficaces pour ces matériaux. L'article suivant met en avant une méthode statique permettant de tracer la caractéristique J(H) d'un échantillon de ferrofluide. La première partie décrit le principe de mesure ainsi que la méthode mathématique mis en jeu. La deuxième présente la manière dont le magnétomètre a été conçu, sa réalisation et sa calibration. Dans une troisième partie, le magnétomètre est testé sur un échantillon solide faiblement perméable. Les résultats obtenus sont alors comparés à une mesure par extraction. Enfin, la dernière partie montre par une simulation numérique que le dispositif est capable de mettre en évidence la nature isotrope ou anisotrope de l'échantillon testé.*

European Journal of Electrical Engineering – n° 5-6/2014, 327-344

KEYWORDS: magnetic characterization of ferrofluids and low permeability materials, instrumentation, magnetometer, static sample.

MOTS-CLÉS : caractérisation magnétique de ferrofluides et matériaux faiblement perméables, instrumentation, magnétomètre, échantillon statique.

DOI:10.3166/EJEE.17.327-344 © Lavoisier 2014

1. Introduction

Ferrofluids are colloidal suspensions of ferromagnetic or ferrimagnetic nanoparticles (Fe_2O_3, Fe_3O_4, Mn-Zn ferrite), suspended in organic solvents or water (Rosenzweig, 1997). Their specific magneto-thermal properties can be used to generate a pressure gradient (Matsuki, 1977; Petit, 2013), thanks to the combined action of a magnetic field and a temperature gradient. Thus the fluid can flow in a closed loop without any mechanical moving part (Petit, 2012; Love, 2005). A magnetothermal pump is then created (Burmundez-Torres, 2007). This type of pump is interesting especially in Power Electronics cooling. The ferrofluid is then the coolant and its circulation is performed without mechanical pump, unreliable device with additional losses.

When ferrofluid is subjected to an external magnetic field, the magnetic particles interact and structure into chains (Petit, 2012; Rosenzweig, 1997). This phenomenon leads to surface instabilities that appear to minimize the magnetostatic energy (Bacri, 1995). Interaction between external field and magnetic particles can affect the viscosity (Odenbach, 2006), the thermal conductivity (Philip, 2007) and the heat transfer coefficient (Cherief, 2014). Also, the formation of chains makes the ferrofluid anisotropic regarding its magnetic properties. Finally, because of their low Curie temperature, the ferrofluid magnetization is sensitive to temperature, and decreases when the operating temperature increases. The design of such a pump is complex given the strong coupling between heat and magnetism, but also because of parasitic coupling. A prerequisite for the optimization is the study of the ferrofluid magnetothermal behavior. A precise characterization of the magnetization and its anisotropy as a function of the field and the temperature should be investigated. Conventional methods as extraction type magnetometers or vibrating sample magnetometers (VSM) require the displacement of the sample. In the case of ferrofluids, this can modify the distribution of particles within the carrier fluid, affecting magnetization. Therefore, a static method in which the sample is fixed is necessary. In addition, these conventional methods are not suited to a simple study of the ferrofluid anisotropy induced by the nanoparticles chains formation.

This paper presents a novel magnetometer suitable to characterize magnetic fluids or low permeability magnetic solids. It can be also used for the analysis of the anisotropy of the material. The measuring principle is described and confirmed by finite element simulations. The practical aspects of implementation and calibration are also presented. A solid SMC sample is used to validate the proposed approach.

Finally, numerical simulations are investigated to show how the device can be extended to quantify the anisotropy behavior of ferrofluids.

This structure of magnetometer has already been put forward in the past (Petit, 2014). However this new article comes in addition to the studies already carried out. Indeed, the study of the anisotropy was raised. This paper shows by finite element simulations and theoretical manner the possibility of studying this characteristic.

2. Magnetometer description

2.1. Measurement principle

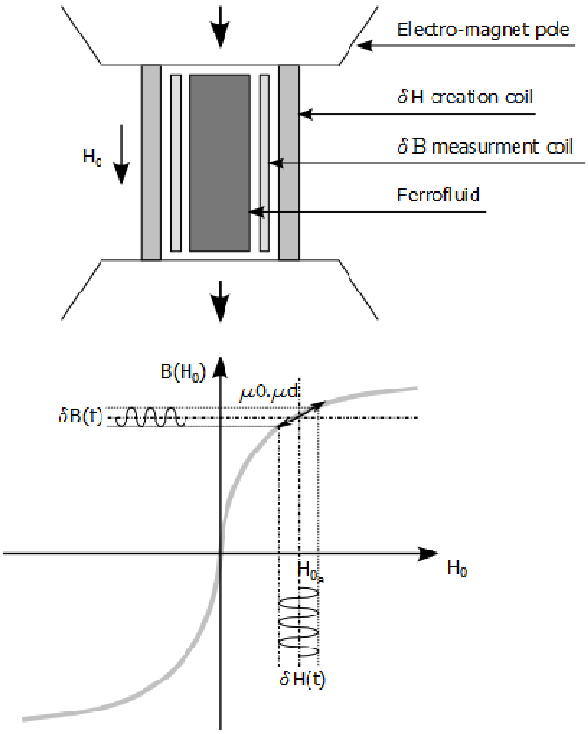

Figure 1. Magnetometer principle

Figure 1 describes the principle of the magnetometer. As the sample should not move, it is submitted to a double excitation: a DC applied field H_0 which is generated by a conventional electromagnet, and measured near the sample by a Hall

probe and an AC low level applied field parallel to H_0. We propose to construct the curve *J(H)* by measuring the differential susceptibility χ_d of the sample in a cylinder with a radius $R_{sample,}$ for different polarization values.

The alternative magnetic excitation is generated by a coil supplied by a sinusoidal current δi at frequency *f*. We note δH the corresponding amplitude of the internal field. As the magnetic circuit is not completely closed, δH value cannot be deduced directly from δi. A suitable circuit devoted to δH and also magnetic induction *B* measurements is then implemented. Its principle is described in more details in the following paragraphs. It is mainly composed of three concentric coils having the same number of turns N and set around the sample.

2.1.1. AC magnetic field measurement

Considering the tangential component conservation at the side surface of the sample, the internal AC field δH can be determined by measuring the field δH_1 in the air at a given distance d_1 from this surface. Assuming that this field does not vary with $d_{1,}$ we can state that $\delta H = \delta H_1$. *It* can be measured using an additional second coil l to the induction measurement coil. These coils are respectively δh_1_Coil and B_Coil. They have the same number of turn noted N and a respective section of S_{h1} and S_b. In practice, δH_1 cannot be obtained directly from the E.M.F. induced in δh_1_Coil because, it is surrounding the sample. A differential measurement of the two detected signals is performed (see Figure 2). Technically, because the external field to the sample is not constant and the size of the coils requires a certain distance R_{h1} - R_{sample} between the air-material interface and the measurement area, the relationship $\delta H = \delta H_1$ is no longer strictly ensured. The accuracy is then improved by measuring two fields δH_1 and δH_2 at two different distances from the sample side surface. A simple linear interpolation allows having a more accurate δH. A third concentric coil with the same number of turn N and S_{h2} section, is then added to the others (see Figure 3). δH_2 is obtained also at the distance R_{h2}, by a differential method between h_2_Coil and h_1_Coil. This method called Double H-coil method is well known and widely used for the characterization of soft magnetic materials by mean of Single Sheet Tester (SST) or Rotational Single Sheet Tester (RSST) (Nencib, 1996). The final magnetic field value is estimated using the following formula:

$$\delta H = \delta H_1 - (\delta H_2 - \delta H_1).\frac{R_{h1}-R_{sample}}{R_{h2}-R_{h1}} \quad (1)$$

Given the "small signal" regime, the magnetic circuit behaves linearly around the operating point determined by the constant field H_0, as shown in Figure 2. The demagnetizing linked to the open geometry of the input circuit then causes no distortion of the waveform, so that the total excitation field itself varies sinusoidally.

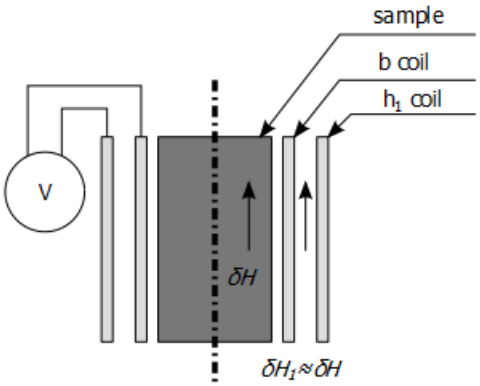

Figure 2. Field measurement principle

The δH_1 and δH_2 RMS values are expressed as a function of the RMS differential voltages $V_{h1\text{-}b}$ and $V_{h2\text{-}h1}$ according to:

$$\delta H_1 = \frac{V_{h1-b}}{\mu_0 \cdot (S_{h1} - S_b) \cdot N \cdot 2\pi \cdot f} \quad (2)$$

$$\delta H_2 = \frac{V_{h2-h1}}{\mu_0 \cdot (S_{h2} - S_{h1}) \cdot N \cdot 2\pi \cdot f} \quad (3)$$

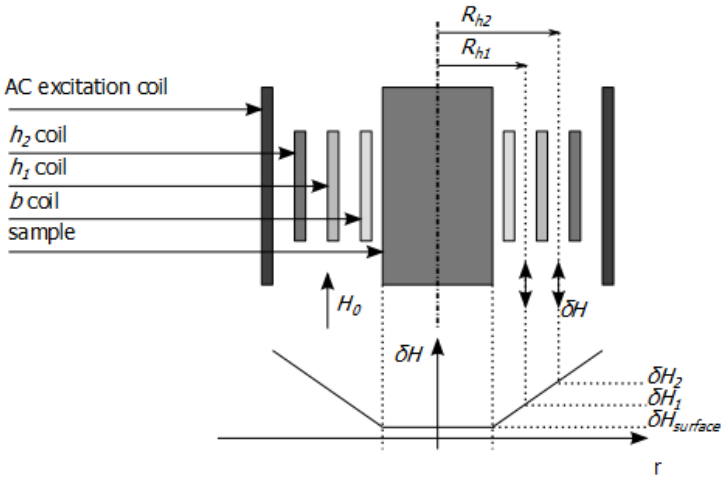

Figure 3. Magnetic field measurement at the surface sample, Double H-coil method

2.1.2. Induction δB measurement and differential susceptibility determination

The b-coil detects the flow through the sample but also the leakage flux in the air portion enclosed by the coil. The induced voltage V_b at the coil terminals is then expressed by Equation (4). A correction is then made considering that, in this region very close to the sample, the field is equal to δH. δB is calculated using Equation (5).

$$V_b = 2.\pi.f.N.S_{ech}.\delta B + 2.\pi.f.N.\left(S_b - S_{sample}\right).\mu_0.\delta H \quad (4)$$

$$\delta B = \frac{V_b}{2.\pi.f.N.S_{sample}} - \mu_0.\delta H.\frac{S_b - S_{sample}}{S_{samle}} \quad (5)$$

By definition, the differential susceptibility χ_d verifies the following equation:

$$\chi_d = \frac{\delta B - \mu_0.\delta H}{\mu_0.\delta H} \quad (6)$$

2.2. J(H) curve reconstruction

The Hall effect sensor measures the static field H_0 in a region close to the sample but in its absence. The internal field H associated to H_0 is affected by a demagnetizing contribution that is made through an equivalent demagnetizing coefficient N_Z tabulated by Chen (Chen, 2006). N_Z depends on the form factor of the sample and the permeability of the material. The field H verifies then:

$$H = \frac{H_0}{1 + \chi.N_z} \quad (7)$$

where $\chi = \frac{J}{\mu_0.H}$ indicates the susceptibility amplitude.

Knowing H and $\chi_d(H)$, the material characteristic curve $J(H)$ can be reconstructed, as shown in Figure 4. This characteristic can be expressed by:

$$J_i = J_{i-1} + \mu_0.\frac{\chi_{d_{i-1}} + \chi_{d_i}}{2 + N_z(\chi_{d_{i-1}} + \chi_{d_i})}.\left(H_{0_i} - H_{0_{i-1}}\right) \quad (8)$$

2.3. Numerical verification of the measurement conditions

Inhomogeneity of H_0 or δH can lead to significant measurement errors. Numerical simulations were performed under FLUX™ software to study this issue and help the design of the magnetometer.

2.3.1. H_0 field homogeneity

The study of the homogeneity of the field H_0 is performed via a 2D axsymmetric simulation. The dimensions of the poles of the electromagnet are taken from R.

Merle PhD (Merle, 1992), who designed it. The homogeneity of the field is verified in the air gap, along different paths and at different induction levels in order to evaluate the effect of the magnetic poles saturation.

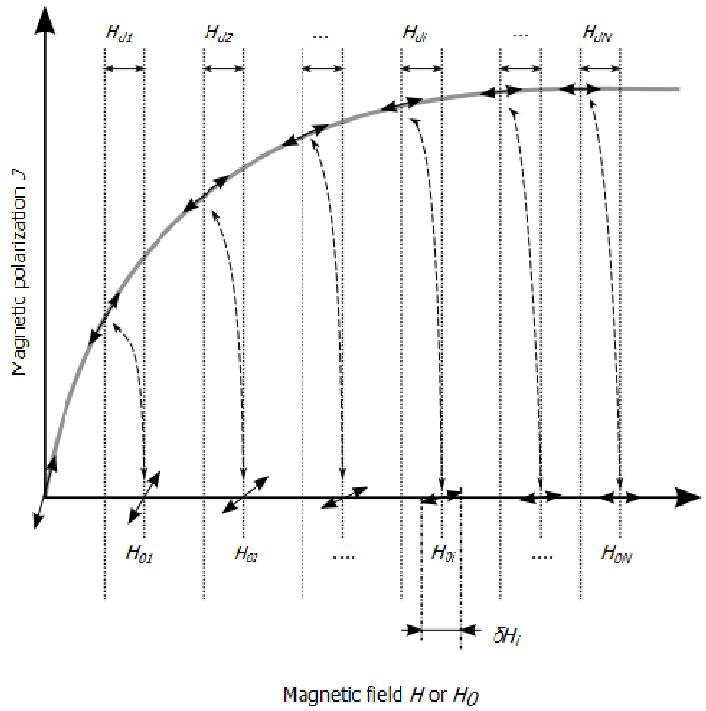

Figure 4. J(H) curve reconstruction principle

In order to simplify the simulations, the flux is imposed, rather than the current, with a zero potential on the symmetry axis.

To account for magnetic leaks at the poles, the boundary of the study area is extended to $R_{boundary}$= 150 mm while the maximum value of cylinder radius associated with the pole is only 80 mm. For simulation the geometry of the pole is simplified and described as an assembly of 3 tapered regions having respectively an inner and outer radius of (22, 35), (35,60) and (60,80) in mm and a height of 2.5, 15 and 348 mm, An effective airgap e = 25 mm is imposed between the two poles.

The vertical component of the applied magnetic flux density B_0 is observed on the different paths, as shown in Figure 5. Path 1 coincides with the vertical axis of symmetry. Path 2 allows to observe the induction on the upper side of the sample.

Finally, path 3 reports on the DC magnetic polarization on the revolution axis of symmetry.

Figure 6 shows the vertical component of B evolution along the different paths and different magnetic flux density in the electromagnet center. The homogeneity is expressed considering the error ε as:

$$\varepsilon(z,r) = \frac{B_z(r,z) - B(0,0)}{B(0,0)} \tag{9}$$

where z = 0 mm for path1, z = 10 mm for path 2. And r = 0 mm for path 3, z is now the variable.

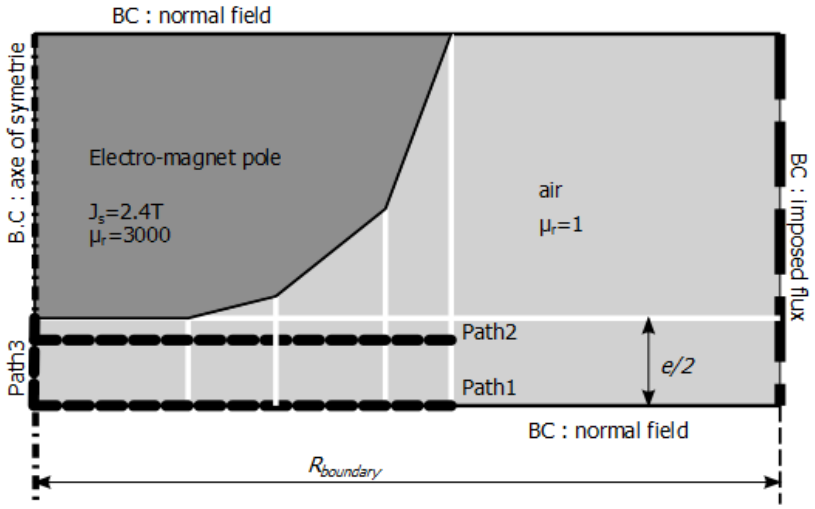

Figure 5. Magnetic field homogeneity verification on different paths (BC: Boundaries Conditions)

The simulated electromagnet was designed to generate a uniform maximal induction of 2T in a volume of 20 mm diameter and 30 mm height (Merle, 1992). The sample dimensions R_{sample} = 5 mm and H_{sample} = 20 mm were chosen accordingly. Along the horizontal paths 1 and 2, the study shows that *B* is uniform within 1% over a distance of 10 mm. We note against a 10% variation of *B* along the symmetry axis. We conclude from these simulations that the field H_0 is quasi homogeneous over the volume occupied by the sample.

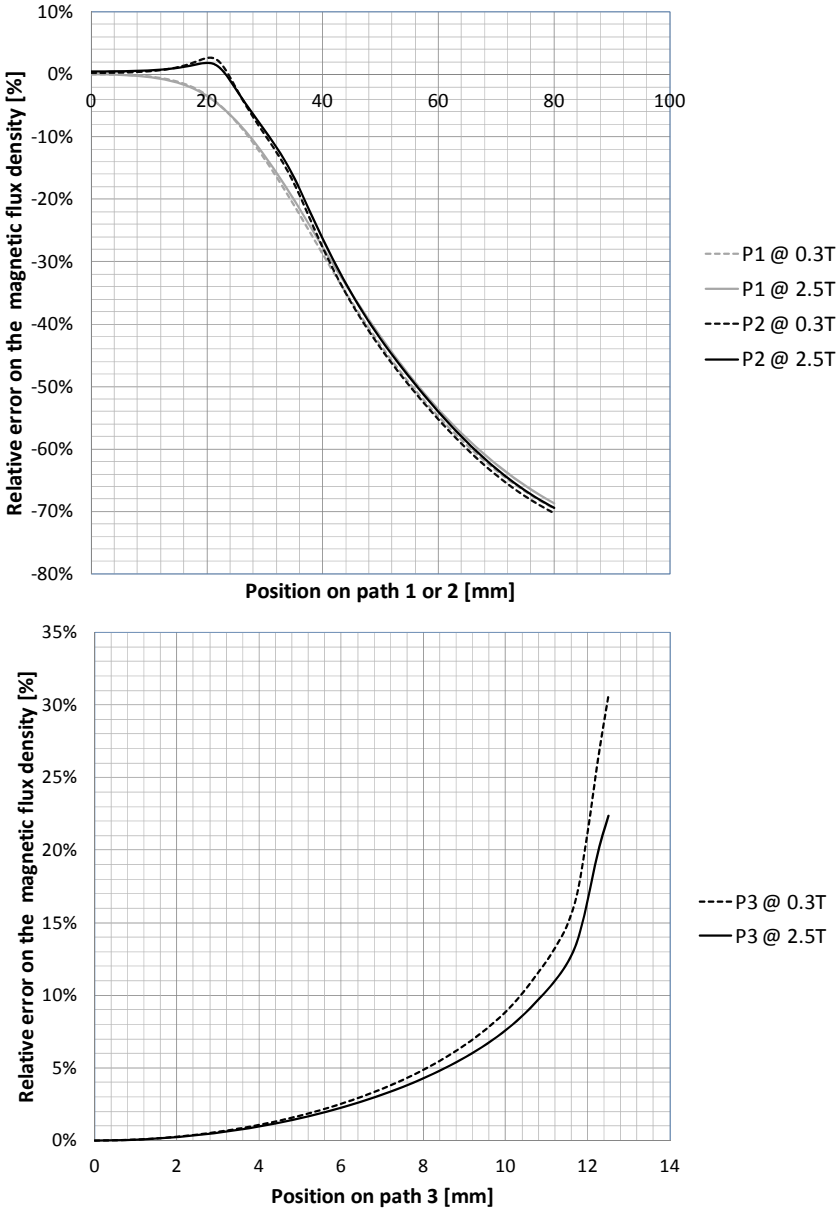

Figure 6. Magnetic field homogeneity verification on different paths

2.3.2. δH field homogeneity

The measurement system is simulated in 2D axisymmetric conditions. The external field H_0 is applied uniformly thanks to an outer coil fed with an adjustable constant current. According the principle of the magnetometer cell, δH is applied by a coil fed by an alternative current. As shown in Figure 7, the resulting δH field is not uniform over the whole height of the sample. That is why only the central part of the sample is considered for the magnetic field measurement. Thus, the measurement coils are 20 mm high while the exciting coil 20 mm.

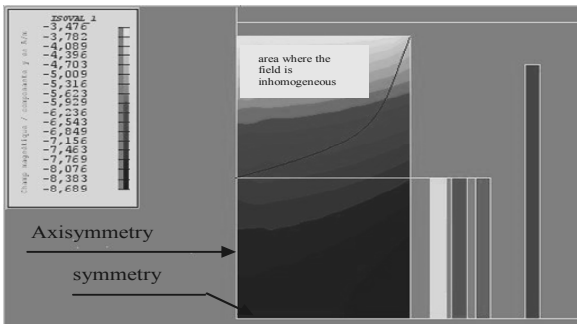

Figure 7. Analysis of the homogeneity of the field δH

3. Experimental setup

3.1. Construction and calibration of the measuring device

Measuring coils (height 10 mm and diameters of 10, 12 and 14 mm for the coils b, h1 and h2) were optimized using simulations.

Special care has been taken to obtain a good sealing of the sample holder. Measuring coils were wound directly thereon to the position closer to the sample. The four coils (excitation, b, h_1 and h_2) were realized successively on each other by interposing thin layers of resin and rigidifying the assembly in a single block. Finally, the numbers of turns are 81 for the measurement coils and 110 in two layers for the excitation coil.

Finally, the sections S_b, S_{h1}, S_{h2} of the measurement coils are determined by a calibration carried out in a 0.05% uniform field generated by a Helmholtz coil system. The coils were subjected to sinusoidal fields of various magnitudes for three frequencies f = 11, 95 and 1095 Hz. Figure 8 illustrates the results obtained for the h_2 coil. In this figure, the ratio of the voltage on the frequency is represented versus the applied magnetic field. All the curves are collinear. The section of the coil can be calculated from any frequency results. Table 1 summarizes the results showing

the average and extreme values. The relative differences, less than 0.5%, are expressed relatively to the average values.

An additional test with an impedance analyzer shows that the magnetometer can be used from 10 Hz to 100 kHz without any disturbance of resonance.

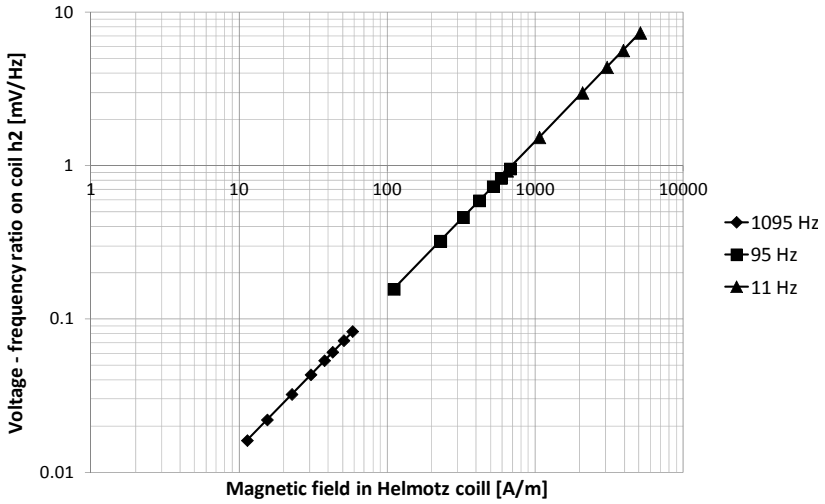

Figure 8. Experimental determination of the section of the h_2-coil

Table 1. Calibration of the magnetometer coils

Coil	S_{Mean} [mm²]	S_{min}[mm²]	S_{max}[mm²]	R[mm]
Excitation	260.2	259.6 (-0.3 %)	261.8 (+0.5 %)	9.10
b	105.0	104.9 (-0.1%)	105.2 (+0.2%)	5.78
h_1	127.97	127.8 (-0.2%)	128.3 (+0.3%)	6.38
h_2	157.4	156.7 (-0.4%)	158.0 (+0.3%)	7.08

3.2. Results using parallel AC and DC polarizations

As mentioned above, the DC field is determined with a Hall probe. AC measurements are carried out at a frequency of 1024 Hz. However, lower and higher frequencies are also tested to verify the behavior of the system. A differential low-noise amplifier (SR560) and a high-precision voltmeter (HP3458A) are used to measure the induced voltages. The δH field is less than 200 A/m and therefore

relatively low. In these conditions, it is assumed that it does not disturb the microstructure of the ferrofluid and chaining induced by the DC field. δB is less than 1 mT.

The magnetometer was initially characterized empty. This test showed a systematic error of about 6%, which affects the differential susceptibility. This is attributed to the deterioration of the homogeneity of the field when no sample is used. The measured permeability μ_{r0} is kept as reference. Each permeability μ_{dmes} measurement is corrected as

$$\mu_d = \frac{\mu_{dmes}}{\mu_{r0}} \tag{10}$$

Only the permeability μ_d is used for the reconstruction of the characteristic curve *J(H)*.

To test the behavior of the magnetometer, a solid sample made with a low permeability material was used. It is a cylinder 9.88 mm in diameter and 20 mm long cut from a soft magnetic composite block. The material consists of 90% by mass of iron powder mixed with a resin and pressed at 400 MPa using an industrial process. Its density is 4.5 g/cm^3 and its saturation polarization J_s is about 0.6 T.

To validate our approach, a second specimen, a cylinder 6 mm in diameter and 6.45 mm in height, was carved in the same block and characterized using a conventional extraction magnetometer from Néel Institute (Grenoble, France). The corresponding measures are considered as the reference.

The results obtained with the two magnetometers are reported in Figure 9. N_Z demagnetizing coefficients are calculated from Chen (Chen, 2006) and are worth 0.165 and 0.290, respectively. These values are average values which are calculated by adopting a susceptibility χ magnitude in the range 0 to 9.

In fact, the use of an average susceptibility may be insufficient. Probably the accuracy could be improved by changing the value of N_Z at each iteration according to the susceptibility χ value obtained in the previous step. A complex procedure would be therefore required because χ, χ_d and N_Z are interdependent. In addition, the measurements are not carried out in practice in a real open circuit because the distance between the sample and the pole pieces of the electromagnet is only several millimeter. This can modify the calculations, especially under high DC induction because the poles can saturate locally. Nevertheless, the results are very satisfactory and validate the proposed magnetometer.

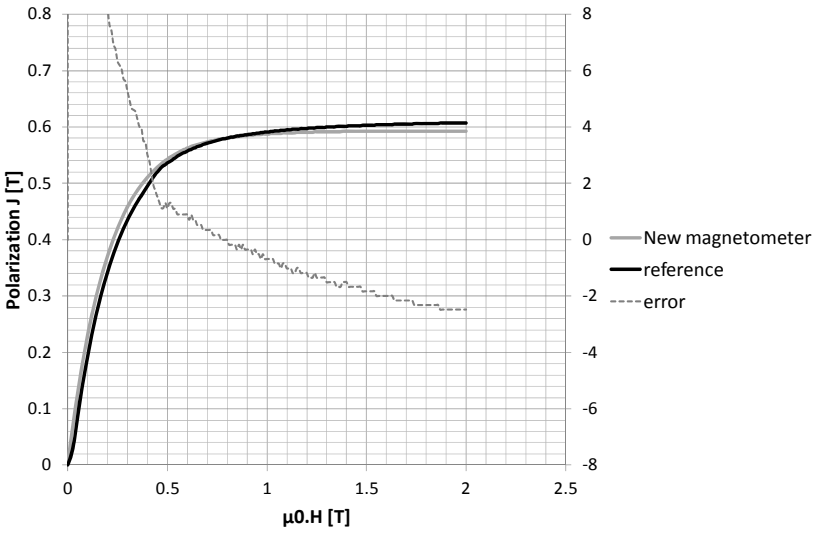

Figure 9. Comparison between the two methods

4. Anisotropy quantification

As said before, a polarized ferrofluid can structure itself into chains. This phenomenon makes ferrofluids anisotropic. The analysis of the susceptibility when the magnetometer cell is perpendicular to the DC magnetic field, as shown in Figure 10 can highlight the anisotropic behavior of the sample.

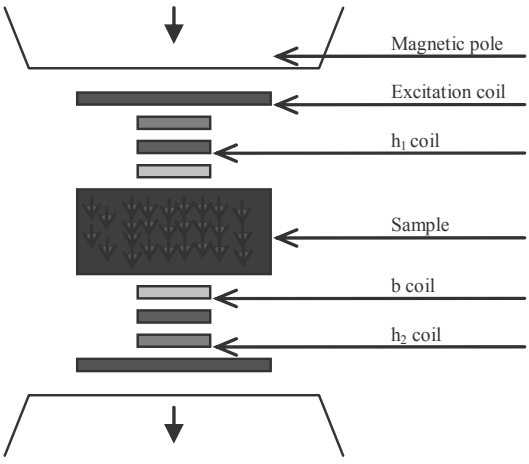

Figure 10. Perpendicular susceptibility measurements configuration

4.1. Perpendicular AC and DC polarizations

Let us consider a magnetized material by a vertical static field H_S. A horizontal sinusoidal excitation δH_h is added. The total field H_t can be written as:

$$H_t = \sqrt{H_s^2 + \delta H_h^2} \tag{11}$$

The angle θ between H_t and δH_h is defined as:

$$\sin\theta = \delta H_h / H_t \tag{12}$$

The material acquires a polarization $J(H_t)$ parallel to H_t. Its horizontal component is noted δJ_h. The horizontal susceptibility $\chi_h = \delta J_h / (\mu_0 \, \delta H_h)$ can be expressed by:

$$\mu_0 \, \chi_h = \frac{J.\sin\theta}{\delta H_h} \tag{13}$$

Combining Equations (12) and (13), the permeability can be expressed as:

$$\mu_0 \, \chi_h = \frac{J}{H_t} \tag{14}$$

This susceptibility χ_h equals the amplitude susceptibility. $J(H_t)$ is therefore the same than $J(H_S)$ if $\delta H_h << H_S$. This is a considerable simplification compared to the parallel configuration.

Finally, note that the demagnetizing coefficient for the measurement is no longer N_Z, the DC bias being no longer aligned with the cylinder axis. The new demagnetizing coefficient is estimated to be 0.42, as shown in Chen Tables (Chen, 2006).

The parallel and perpendicular configurations allow to reconstruct a curve $J(H)$. If the material is isotropic, the reconstruction leads to an identical curve in both directions. If the material is anisotropic, for example in a polarized ferrofluid, the two curves are different.

4.2. Verification of the principle by F.E.M. simulations

The perpendicular configuration breaks the rotational symmetry. The simulations are thus performed in 3D. To simplify the study, we do not include the effects of the electromagnet poles. The sample and the AC coils (excitation and measurements) are set in the center of a DC coil generating an induction B_0 adjustable up to 2 T. To obtain a homogeneous simulated field, we impose on the outer surface of the DC coil a boundary condition of tangential magnetic field. The boundary condition on the upper and lower surfaces is a normal magnetic field. In this arrangement, shown

in Figure 11, the susceptibility is measured by the magnetometer, and the applied field is estimated near the magnetometer, on the coil axis.

In this simulation, the material behavior is assumed and is expressed by:

$$J(H) = \frac{2.J_s}{\pi}.\text{atan}\left(\frac{\pi.\mu_0.(\mu r_i - 1).H}{2.J_s}\right) \tag{15}$$

where J_s is the saturation polarization and μ_{ri} is the initial relative permeability. These values are set to 0.4 T and 5.

In order to compare the parallel and perpendicular configurations, the two simulations have been performed.

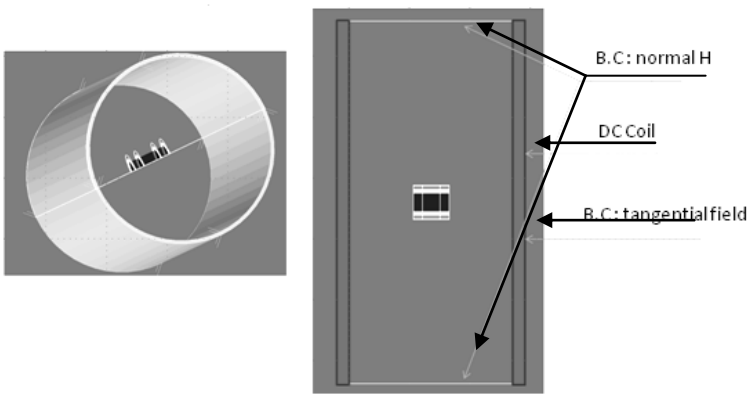

Figure 11. Simulation geometry in the perpendicular case

Figure 12 shows the simulation results and compares the theoretical values (solid lines) of μ_{rd} differential (gray) and μ_r amplitude (black) relative permeabilities obtained according to Equation (7) with their values reassessed by simulation. The theoretical and simulated curves have the same shapes but are significantly different from the quantitative point of view. There is the problem associated with low susceptibility mentioned in § 3.2, the susceptibilities measured values pretend never tend towards 0. A recalibration of the measured quantities is required. It is performed in the same manner as in § 3.2. A first relative permeability μ_{r0} is measured by an unload magnetometer test. μ_{r0} is less than 1. This measurement error comes from the inhomogeneity of the magnetic field in the sample. This error is systematic, and is compensated: each measurement must be divided by the empty test relative permeability. Figure 12 present the final corrected results

Knowing the differential and amplitude permeability, it is easy to reconstruct the two curves *J(H)* associated with the perpendicular and parallel configurations. The comparison of these two curves shows then if the material is isotropic or not.

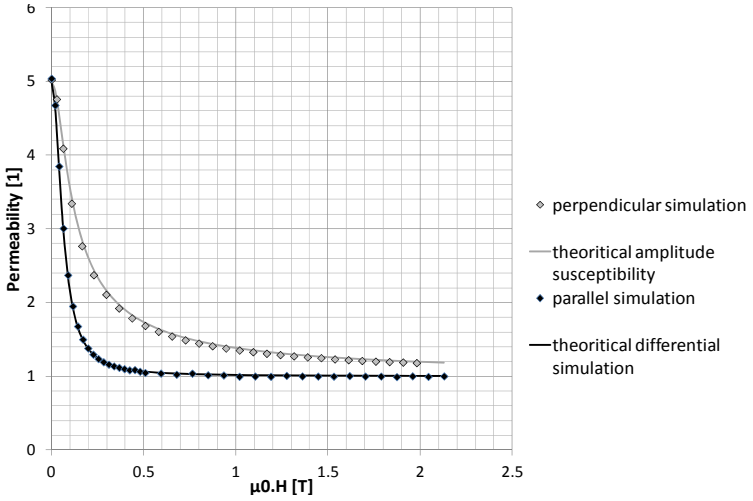

Figure 12. Theoretical and numerically measures of differential and amplitude permeabilities

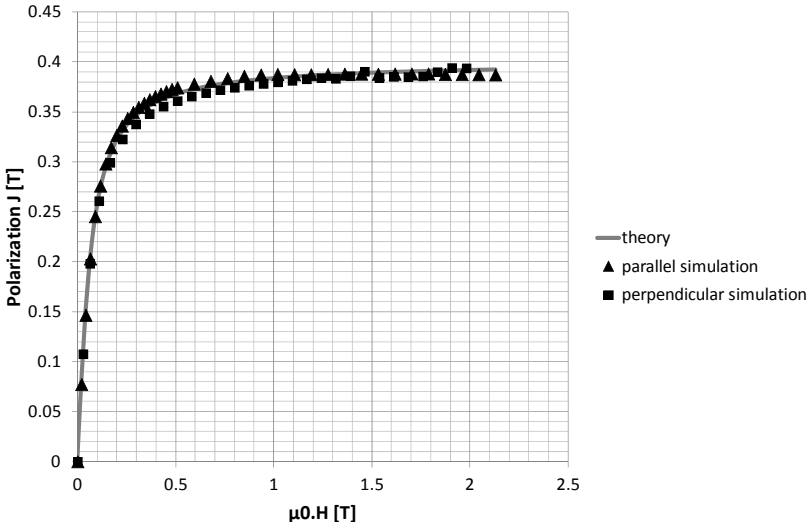

Figure 13. Comparison of theoretical and simulated curves J(H) obtained by the two methods

3D simulations presented in Figure 11, have a mesh default. Indeed, the space between the different coils of the magnetometer and the sample is small regarding the dimension of the system. This space and the coils must be meshed in parallelepipeds while the rest of the geometry is meshed with prisms. The junction between parallelepipeds and prisms can produce some disturbance in the Maxwell's equations resolution. In addition, 3D simulations cannot allow a very dense meshing without increasing dramatically the simulation times. Thus, the meshing size was increased to limit the simulation time.

All these small defects lead to numerical noise, which can explain the discrepancies between the simulations results and the theoretical values shown in Figure 13. However, these simulations prove the validity of the proposed methods.

5. Conclusion

A magnetometer adapted to the characterization of ferrofluids or low permeability materials has been developed. The device is based on an indirect determination of the curve *J(H)*. The principle considers the measurements of the differential susceptibility at different bias fields generated by an electromagnet. The *J(H)* curve is then reconstructed point by point. Finite element simulations performed for linear and nonlinear materials are used to validate the design of the magnetometer. A double H-coil method is investigated to improve the measurement accuracy.

Once the magnetometer built and calibrated, an experimental validation on a low permeability composite was carried out. The results were compared with those given by an extraction magnetometer. These results show that the developed magnetometer and the proposed technique for the reconstruction of the curve *J(H)*, allow to correctly obtain the material behavior. The magnetometer as well as the evaluation of the demagnetizing coefficient can be improved, but the estimation error remains lower than 5%, which is generally sufficient to characterize the ferrofluids.

A second step of this work was to demonstrate the feasibility of the measure in the transverse direction, *via* F.E.M. simulations. In this case, the reconstruction is not necessary since the measurement provides a direct calculation of the susceptibility of amplitude. It is then possible to reconstruct two characteristic curves *J(H)*, one in the direction of H_0 and the other in the perpendicular direction. The comparison of these two curves can be used to identify the isotropic or anisotropic nature of the sample.

The next stage of our work will be an experimental validation of the measurement principle in the transverse direction. First, the same solid and isotropic sample will be tested. Then a same analysis will be achieved with a known

anisotropic material. Finally a low concentration ferrofluid will be characterized along the longitudinal and transverse direction.

Acknowledgments

The authors thank the Néel Institute for providing the extraction magnetometer and Morgan Almanza, PhD student at G2Elab for characterizing the reference composite sample.

References

Burmundez-Torres E. (2007). *Design and mechanical characterization of a magnetocaloric pump*. Thèse en mécanique University of Puerto-Rico.

Bacri J.C. (1995). *Liquides magnétiques ou ferrofluides* (éd. ref D2180). Paris: Edition T.I.

Cherief W. (2014). Intensification des transferts de chaleur, par convection forcée en cuite de section carrée avec des ferrofluides, *Acte de congrès, SGE* 2014, Cachan.

Chen D.X. (2006). Fluxmetric and magnetometric demagnetizing factors for cylinders, *J. Mag. Mater*. 306, p. 135-146.

Love L.J. (2005). Ferrofluid field induced flow for microfluidic applications. *IEEE Transactions on Mechatronics*, vol. 10, n° 1, p. 68-76.

Matsuki H. (1977). Experimental considerations on a automatic cooling device using temperature-sensitive magnetic fluid, *IEEE Transactions on Magnetics* , vol. 13, p. 114-1145.

Merle R. (1993). *Utilisation des aimants Néodyme-Fer-Bore dans les Machines électriques*, Thèse en Génie Electrique, INPG, Grenoble, 1993.

Nencib N. (1996). Performance evaluation of a large rotational single sheet tester, *J. Mag. Mag. Mater*. 160, p. 174-176

Odenbach S. (2006). *Handbook of magnetic material,* (éd. Elsevier), Elsevier Science.

Petit M. (2013). Experimental study of a static system based on a magneto-thermal coupling in ferrofluids. *International Journal of Refrigeration*, vol. 37, p. 201-208

Petit M., Kedous-Lebouc A., Avenas Y., Cherief W., Rulliere E. Anceau B. (2014). Static Sample Magnetometer: A New Characterization Method for Low Permeability Materials and Ferrofluids. *Magnetics, IEEE Transactions on*, vol. 50, n° 4, p. 1-4, April.

Petit M. (2012). Contribution à l'étude des systèmes de refroidissement basés sur le couplage magnéto-thermique dans les ferrofluides à faible température de Curie, Thèse en Génie Electrique, Université de Grenoble.

Philip J. (2007). Enhancement of thermal conductivity in magnetite based nanofluid due to the chainlikes structures, *Appl. Phys. Lett*., vol. 91, p. 203108

Rosenzweig R. (1997). *Ferrohydrohynamics,* Ed. Courier Dover Publication, Dover, Courier Dover Publication.

Received: 4 March 2015
Accepted: 15 September 2015